Journal of the Taiwan Institute of Chemical Engineers 93 (2018) 184–192

Contents lists available at ScienceDirect

Journal of the Taiwan Institute of Chemical Engineers

journal homepage: www.elsevier.com/locate/jtice

Advanced photocatalytic Fenton-like process over biomimetic hemin-Bi_2WO_6 with enhanced pH

Huan Yi[a,b,1], Min Jiang[a,b,1], Danlian Huang[a,b,1], Guangming Zeng[a,b,*], Cui Lai[a,b,*], Lei Qin[a,b], Chengyun Zhou[a,b], Bisheng Li[a,b], Xigui Liu[a,b], Min Cheng[a,b], Wenjing Xue[a,b], Piao Xu[a,b], Chen Zhang[a,b]

[a] College of Environmental Science and Engineering, Hunan University, Changsha, Hunan 410082, China
[b] Key Laboratory of Environmental Biology and Pollution Control, Ministry of Education, Hunan University, Changsha, Hunan 410082, China

ARTICLE INFO

Article history:
Received 19 February 2018
Revised 29 May 2018
Accepted 28 June 2018
Available online 27 July 2018

Keywords:
Bi_2WO_6
Biomimetic
Hemin
Photocatalytic Fenton-like process

ABSTRACT

Highly-efficient technologies are urgently needed to remove environmental organic pollutants. Photocatalytic degradation and Fenton (-like) process are often used to remove organic pollutants. But simplex photocatalysis is a rather slow process, while Fenton-like process is often limited by low pH levels. Introducing photocatalysis into Fenton-like process to form photocatalytic Fenton-like system is a promising method to overcome these drawbacks. This work investigated a simulated-solar light (SSL) driven photocatalytic Fenton-like process with using a novel biomimetic photocatalyst hemin-Bi_2WO_6 induced by H_2O_2 (SSL/H-Bi_2WO_6/H_2O_2 process) to degrade organic pollutants. H-Bi_2WO_6 possesses lower fluorescence intensity and faster electron transport than pristine Bi_2WO_6. Additionally, combined experimental and theoretical investigations indicated that SSL/H-Bi_2WO_6/H_2O_2 process revealed a high catalytic activity with enhanced pH tolerance. Furthermore, trapping experiments and electron spin resonance tests were used to explore the reaction mechanism of photodegradation. Presumably, the degradation of organic pollutants over SSL/H-Bi_2WO_6/H_2O_2 process was ascribed to ·OH, h^+, and $\cdot O_2^-$ radical species, and Fe(IV)=O active species generated from the interaction of H_2O_2 with the variable valence state of iron on H-Bi_2WO_6. Overall, this work puts forward a new possibility for aqueous organic pollutants removal via SSL/H-Bi_2WO_6/H_2O_2 process, which may promote the application of photocatalytic Fenton-like process and biomimetic catalysis.

1. Introduction

In recent few decades, environmental pollution is becoming a worldwide environmental issue, especially water pollution caused by organic pollutants with visible, toxic, or nonbiodegradable properties [1–6]. Compared with adsorption process [7–11], conventional oxidation process [12,13], biotreatment [14–17] and electrochemical process [18], photocatalytic degradation and Fenton-like process have been widely applied in the treatment of organic pollutants [19–22]. But simplex photocatalysis or Fenton-like process has some drawbacks that limit their efficiency in the removal of organic pollutants. Photocatalysis is a rather slow process due to its low oxidation rate, while Fenton-like process alone is often limited in working at low pH levels to avoid catalyst precipitation [23,24]. These drawbacks restrain the practical applications of these individual methods to dispose organic pollutants economically [25]. Thus, the introduction of photocatalysis into Fenton-like process to form photocatalytic Fenton-like system is presented for the removal of organic pollutants, which may improve catalytic activity and pH tolerance.

Some semiconductors have been reported to combine with Fenton-like reaction to show an effective degradation of organic pollutants, such as carbon nanodots [26], TiO_2 [27], g-C_3N_4 [28,29], and WO_3 [30]. Compared with these semiconductors, Bi_2WO_6 shows remarkable photocatalytic activity when combined with Fenton-like process owing to its layered structure and narrow band gap [31–36]. Combining with Fenton-like process show the potential to solve the high recombination of photoexcited electron-hole pairs in photocatalytic process with using Bi_2WO_6 alone [37,38]. In traditional Fenton (-like) process, iron ions were the usual Fenton reagent used for H_2O_2 activation, which has several main disadvantages [39–41]: (i) production of additional iron sludge with increased pH; (ii) limitation of the activity by pH levels;

* Corresponding authors at: College of Environmental Science and Engineering, Hunan University, Changsha, Hunan 410082, China.
E-mail addresses: zgming@hnu.edu.cn (G. Zeng), laicui@hnu.edu.cn (C. Lai).
[1] These authors contribute equally to this article.

https://doi.org/10.1016/j.jtice.2018.06.037
1876-1070/

(iii) secondary pollution with excessive use; (iv) difficulties in catalysts reuse; (v) increased cost for industrial disposition of iron sludge. So in this study, hemin, a biologically active metalloporphyrin complex, was chosen as the Fenton-like reagent modified on Bi_2WO_6 surface to avoid these disadvantages. Hemin has been widely explored as a biomimetic catalyst in the last few years owing to the unique photochemical behavior and biological value [42–44]. For example, a biomimetic photocatalytic system over the combined g-C_3N_4-IMD-hemin with the assist of H_2O_2 revealed high photocatalytic oxidation activity [45] and a prepared hemin-functionalized graphene hydrogel showed strong antibacterial properties [46]. The enhanced photocatalytic activity might be contributed to the sensitization with the hemin, which can improve the separation of photoexcited electron-hole pairs [47]. On the other hand, hemin molecules are easy to aggregate in aqueous solutions [48]. Combining with Bi_2WO_6 that acting as a support might be a feasible way to solve the aggregation problem, and then prevent the generation of inactive dimers and oxidative self-destruction of hemin in the photochemistry system.

Hydrogen peroxide is a key factor in the photocatalytic Fenton-like system. H_2O_2, an inorganic oxidant with a standard potential of 2.84 V verses standard hydrogen electrode, has a significant rate-enhancing effect on the degradation of organic pollutants [49]. H_2O_2 is used as a "green" oxidant in organics degradation because (i) it generates H_2O as the only by-product, (ii) it generates active oxygen species, and (iii) it possesses an oxidative potential prevailing to molecular oxygen (1.76 V vs 0.695 V) [50]. In such photocatalytic Fenton-like process, H_2O_2 plays as a powerful scavenger to capture the photogenerated electrons when photocatalysis and Fenton-like process are conducted simultaneously, which can increase the quantum efficiency of this system and accelerate the transport of photoexcited charge carriers and the generation of active species, such as hole (h^+), superoxide radicals ($\cdot O_2^-$), and hydroxyl radicals ($\cdot OH$), for the more efficient removal of organic pollutants [51]. However, a high H_2O_2 concentration was used in many presented wastewater disposal processes, which is not suitable to be used in commercial large-scale application [52,53]. Thus, an effective process with a small amount of H_2O_2 for organic pollutants degradation is urgently needed. And the use of H_2O_2 in photocatalytic Fenton-like process must be examined carefully, because there may appear negative effects with a too low or too high H_2O_2 concentration. Moreover, few documents investigated the effect of pH on the combined photocatalytic Fenton-like process. Hence, the effect of pH on photocatalytic Fenton-like process needs to be further study.

This work combined an environment-friendly biomimetic material hemin and a low-cost photocatalyst Bi_2WO_6 together to get a novel hemin modified Bi_2WO_6 (H-Bi_2WO_6) composite via a facile solvothermal method. The morphology and optical properties of H-Bi_2WO_6 samples were systematically characterized by the field emission scanning electron microscopy (FESEM), transmission electron microscopy (TEM), X-ray diffraction (XRD), X-ray photoelectron spectroscopy (XPS), UV–vis diffuse reflection spectroscopy (DRS) and photoluminescence (PL) spectroscopy. Rhodamine B (RhB) was chosen as the initial treated organic pollutant to explore the catalytic degradation performance of H-Bi_2WO_6, because RhB is not only a widely used organic dye in industry but also a model pollutant to explore the photocatalytic performance of BWO in many studies [54–57]. A combined experimental and theoretical investigation of the influencing factors in the photocatalytic Fenton-like process over H-Bi_2WO_6 induced by a small amount of H_2O_2 under simulated solar-light irradiation (SSL/H-Bi_2WO_6/H_2O_2 process) was performed, including the effect of different systems, different initial H_2O_2 concentrations, and pH levels. Subsequently, radicals trapping experiment and electron spin-resonance spectroscopy (ESR) analysis technology was performed to probe the generated active species and investigate the possible reaction mechanism in the catalytic degradation over SSL/H-Bi_2WO_6/H_2O_2 process. It is anticipated that the photocatalytic Fenton-like process over SSL/H-Bi_2WO_6/H_2O_2 system has the potential to promote the efficiency of other organic pollutants wastewater treatment.

2. Experimental

2.1. Chemical materials

$Na_2WO_4{\cdot}2H_2O$ (>99.5%) was supported by Tianjin Kaidahua Reagent Co., Ltd (Tianjin, China). Hemin (>97%) was purchased from HeFei BoMei Biotechnology Co.Ltd (Anhui, China). Other chemicals were purchased from Sinopharm Chemical Reagent Co., Ltd (Shanghai, China). De-ionized water (18.25 MΩ cm) was used in the whole experiment.

2.2. Preparation of catalysts

Bi_2WO_6 was prepared through hydrothermal method [58]. H-Bi_2WO_6 was prepared from hemin and obtained Bi_2WO_6 samples through one-step solvothermal process. In a typical procedure, 20 mg of hemin and 200 mg of Bi_2WO_6 were first dispersed in acetonitrile and dimethyl sulfoxide mixture (1:1 in volume) to form suspension. The suspension was next stirred at ambient temperature for 30 min, followed by sonication for additional 30 min. The suspension was then transferred to a reaction kettle vessel and heated to 140 °C for 4 h. After cooling to the room temperature, H-Bi_2WO_6 was obtained.

2.3. Characterization

The specific surface area, pore volume and pore size of hemin-Bi_2WO_6 were measured by the Brunauer–Emmett–Teller (BET) adsorption method (Belsorp-Mini II analyser, Japan). PL spectra was recorded with Hitachi F-7000 fluorescence spectrophotometer at an excitation wavelength of 365 nm. The Fourier transforming infrared spectrum (FT-IR) analysis was performed on NICOLET 5700 FT-IR spectrometer. The DRS were performed on Hitachi U4100 UV spectrophotometer. The crystal phase of the samples was determined by using a D/max-2500 XRD (XRD-6100, Japan) with Cu $K\alpha$ radiation ($\lambda = 0.15406$ nm) in the region of 2θ from 10° to 80°. XPS of the samples was obtained by using an ESCALAB 250Xi spectrometer (Thermo Fisher, USA) with Al Kα radiation ($h\nu = 1486.6$ eV). Their morphology was examined by TEM (JEM-3010, Japan). The light irradiation source was a 300 W Xe arc lamp (CEL-HXF300, Beijing). The total organic carbon (TOC) was tested to analyse the mineralization degree of organic dyes on Analytik Jena AG (Multi N/C 2100).

2.4. Photocatalytic activity test

Photocatalytic removal of RhB was carried out under visible light irradiation using a 300 W Xe lamp (CELHXF300, China). In each experiment, 10 mg of photocatalyst was dispersed into 100 mL of RhB solution (10 mg/L). Before irradiation, a certain amount of minutes of dark stirring at room temperature was maintained for achieving the adsorption-desorption equilibrium between the catalyst and RhB. Then the solution pH level was adjusted and a certain amount of H_2O_2 was added before irradiation. Except the experiments of testing the effect of initial H_2O_2 concentrations, 0.5‰ (in volume) of H_2O_2 was added. And all the experiments did not adjust the pH except the tests the effect of pH levels. After that, the mixture was exposed to simulated solar-light, and 3 mL of solution was taken out at given time interval. The residual RhB content of

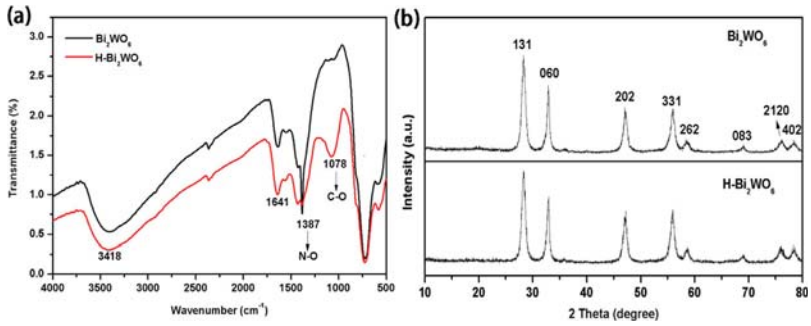

Fig. 1. (a) The Fourier transforming infrared spectrum analysis; (b) XRD analysis of Bi_2WO_6 and H-Bi_2WO_6.

the solution was analysed by a Shimadzu UV–vis spectrophotometer with the absorbance at the characteristic band of 550 nm. Each experiment for photocatalytic measurement were repeated three times.

2.5. Photo-electrochemical measurements

The photocurrent density and electrochemical impedance spectroscopy (EIS) spectra were determined in a conventional three-electrode electrochemical cell with a working electrode, a platinum wire counter electrode and a saturated calomel electrode (SCE) as reference electrode. The working electrode was immersed in a sodium sulfate electrolyte solution (0.5 M) using CHI760E workstation and irradiated at a visible light.

2.6. Active species trapping tests

The active species trapping introduced ethylenediaminetetraacetic acid disodium salt (EDTA-2Na), benzoquinone (BQ), and tert–butyl alcohol (TBA) as the scavengers to detect the effect of h^+, $\cdot O_2^-$, and ·OH in RhB degradation of the photocatalytic Fenton-like system, respectively. The test was performed by 1 mM scavengers to degrade RhB in an aqueous solution over SSL/H-Bi_2WO_6/H_2O_2 process.

3. Results and discussion

3.1. Characterization of the as-prepared H-Bi_2WO_6 photocatalysts

Direct evidence for H-Bi_2WO_6 formation was obtained by FT-IR, XRD and XPS. The FT-IR analysis of Bi_2WO_6 and H-Bi_2WO_6 are shown in Fig. 1a. Main absorption bands at 400–1000 cm^{-1} can be ascribed to the stretching of Bi-O, W-O and W-O-W of Bi_2WO_6. The obvious absorption at 1387 cm^{-1} can be ascribed to N–O bending vibration, which was caused by $NO_3^-$from the raw material HNO_3. The absorption at 1641 and 3418 cm^{-1} are attributed to the bending and stretching vibrations of the adsorbed H_2O molecules, respectively. Compared with the spectrum of Bi_2WO_6, the spectrum of H-Bi_2WO_6 changed at the range of 800–1300 cm^{-1}. The absorption at 1078 cm^{-1} belongs to the C–O stretching, which was attributed to the binding of hemin. These results are consistent with the previous reports [59].

The XRD patterns of Bi_2WO_6 and H-Bi_2WO_6 were also investigated, and the results are revealed in Fig. 1b. It can be seen that there is no change of the XRD pattern from Bi_2WO_6 to H-Bi_2WO_6. All of them demonstrated a typical Bi_2WO_6 crystal structure. The peaks at 2θ around 28.3°, 32.7°, 47.1°, 55.8°, 58.5°, 69.1°, 76.1°, and 78.3°, are attributed to the (131), (060), (202), (331), (262), (083), (2120), and (402) crystallographic planes (JCPDS, No. 39−0256), respectively. Results demonstrated that hemin did not influence the crystal structure of Bi_2WO_6.

XPS experiments were used to demonstrate the formation of covalent bonds during the fabrication of H-Bi_2WO_6. The results of C 1 s, O 1 s, Fe 2p, Bi 4f, and W 4d were presented in Fig. 2. Binding energies are assigned to C, N, O, Fe, Bi, and W (Fig. 2a). Two strong peaks at 159.25 and 164.58 eV of the high resolution Bi 4f XPS spectra (Fig. 2b) are the binding energies of Bi 4f7/2 and Bi 4f5/2, respectively. The high resolution C 1 s XPS spectra are also shown in Fig. 2c with a binding energy at 284.8 eV for C–C/C = C bonds, at 286.1 eV for C–N bonds and at 288.2 eV for C–O bonds. Fig. 2d shows the XPS spectrum in the O 1 s region with a binding energy at 530.4 eV for Bi-O bonds. The XPS spectra from a wide scan indicated the presence of Fe and N. The peak of Fe 2p spectra (Fig. 2e) loaded at 710.38 eV and 723.48 eV are assigned to the energies of Fe 2p3/2 and Fe 2p1/2, respectively, which can be ascribed to the iron atom of hemin. And the peak of N 1 s spectra loaded at 400.0 ± 0.2 eV (Fig. 2a) attributes to the four chemically equivalent N atoms that bind to the central iron atom in hemin [60]. In Fig. 2f, the W 4f spectra of H-Bi_2WO_6 at 35.5 eV and 37.5 eV are assigned to the binding energies of W 4f7/2 and W 4f5/2, respectively. According to all the above results, hemin was successfully modified on Bi_2WO_6 surface.

Furthermore, the morphology of Bi_2WO_6 and H-Bi_2WO_6 has been characterized by SEM and TEM images. Fig. 3a showed the SEM images of Bi_2WO_6, while Fig. 3b and c showed the SEM images of H-Bi_2WO_6. It can be seen that the sample has randomly distributed clusters because of the introduction of hemin on Bi_2WO_6 surface. These surface clusters existing on the H-Bi_2WO_6 can provide many active sites and improve mass transportation, which can further utilize the advantages for photocatalytic degradation. TEM images of H-Bi_2WO_6 (Fig. 3d, e and f) showed that the edge of H-Bi_2WO_6 samples was square laminar. Fig. S1 showed the EDS analysis of the as-prepared H-Bi_2WO_6, which demonstrated that hemin was successfully combined with Bi_2WO_6. Besides, nitrogen adsorption-desorption isotherms experiments were used to further study the surface morphology and pore volume of H-Bi_2WO_6. The results showed that H-Bi_2WO_6 had a little decrease of surface area and pore volume compared with Bi_2WO_6 (Table S1 and Fig. S2).

3.2. Optical property, photoluminescence, and photo electrochemical properties

H-Bi_2WO_6 possessed higher optical absorption than Bi_2WO_6 according to UV–vis DRS (Fig. 4a). PL spectra were recorded to explore the behavior of photoinduced charge carries, and the results suggested the reduced recombination rate of photogenerated electron-hole pairs and the facilitated electron transport and charge-separation efficiency (Fig. 4b). The result of transient photocurrent measurement showed the increased transient photocurrent (Fig. 4c), suggesting the effective separation of photogenerated electron-hole pairs of H-Bi_2WO_6 [61]. EIS is also a method

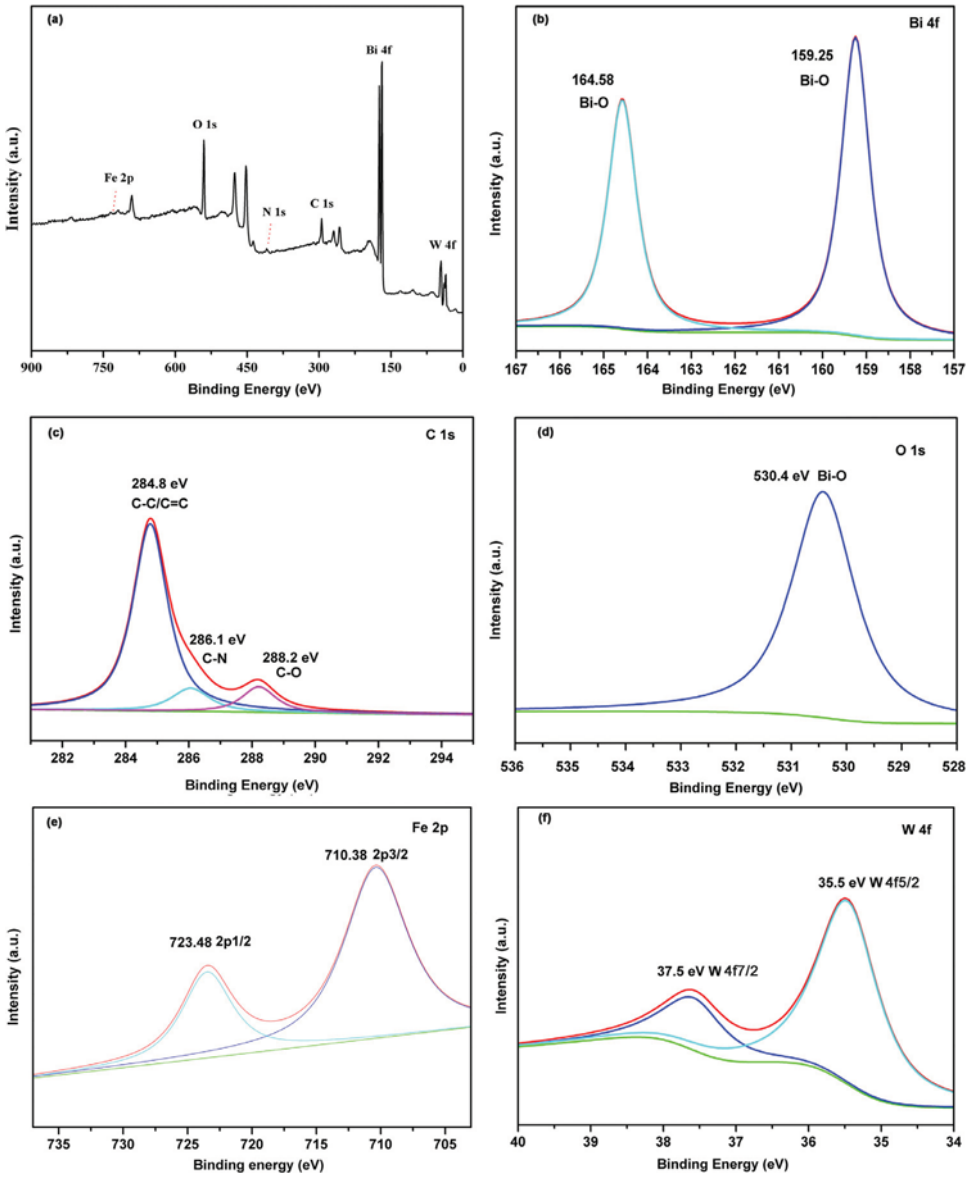

Fig. 2. The XPS analysis of H-Bi_2WO_6: (a) survey spectra, (b) Bi 4f, (c) C1s, (d) O 1s, (e) Fe 2p, (f) W 4f.

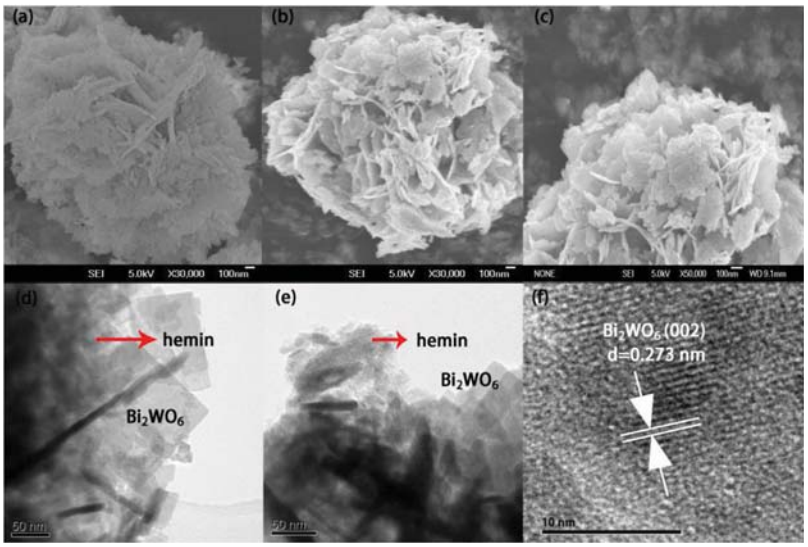

Fig. 3. (a) FESEM images of Bi_2WO_6; (b), (c) FESEM images of H-Bi_2WO_6; (d), (e) and (f) TEM images of H-Bi_2WO_6 from different regions.

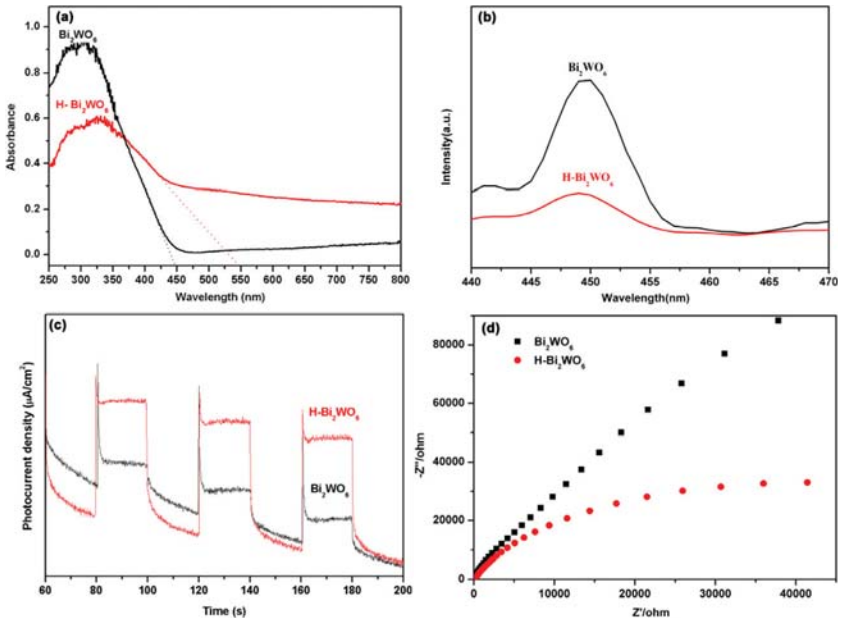

Fig. 4. Optical property, photoluminescence, and photo electrochemical properties analysis of Bi_2WO_6 and H-Bi_2WO_6: (a) DRS; (b) PL; (c) IT; (d) EIS.

to explain the electron-transfer efficiency at the electrodes. The arc radius on the EIS Nyquist plot of the ITO/H-Bi_2WO_6 film was smaller than that of the ITO/Bi_2WO_6 film (Fig. 4d), showing a high electron-transfer efficiency. All of these results revealed a rapid transfer of interfacial charge, and then leading to a valid inhibition in recombination of photogenerated electron-hole pairs.

3.3. Evaluation of photocatalytic activity

A series of experiments were performed to explore the effect factors, including different systems, initial H_2O_2 concentrations (0.2‰–0.9‰ in volume), and pH levels (3, 4, 5, 7, 9, 11, 12, and 13), and the stability of H-Bi_2WO_6. The photocatalytic activities of Bi_2WO_6 and H-Bi_2WO_6 samples were evaluated by the decomposition of RhB under simulated solar-light irradiation. According to the result of RhB adsorption experiments (Fig. S3), the little decrease in surface area and pore volume of H-Bi_2WO_6 had a very small effect on the adsorption capacity, and 30 min dark stirring was maintained for achieving the adsorption-desorption equilibrium between catalyst and RhB. RhB content of the solution was analyzed via UV–vis spectrophotometer with the absorbance at the characteristic band of 550 nm. Besides, TOC analysis was used to measure the mineralization for RhB.

3.3.1. Effect of different systems

Degradation experiments of RhB were performed to explore the catalytic activity of different process. The results are shown in Fig. 5a. Little RhB was removed in SSL/H_2O_2 or SSL/hemin/H_2O_2 process. In SSL/Bi_2WO_6/H_2O_2 process, about 63.7% of RhB was removed in 60 min. And about 71.4% of RhB was removed in the presence of hemin, Bi_2WO_6 and H_2O_2 under SSL irradiation, which was close to the degradation result of SSL/Bi_2WO_6/H_2O_2 process. In contrast, 99.5% of RhB was removed in SSL/H-Bi_2WO_6/H_2O_2 process. The above experimental results demonstrated that the catalytic activity of SSL/H-Bi_2WO_6/H_2O_2 system was higher than other systems.

3.3.2. Stability of prepared H-Bi_2WO_6

H-Bi_2WO_6 samples was performed four reaction runs under the same conditions to test the stability. Comparing fresh and aged H-Bi_2WO_6, nearly no significant loss of catalytic activity was observed

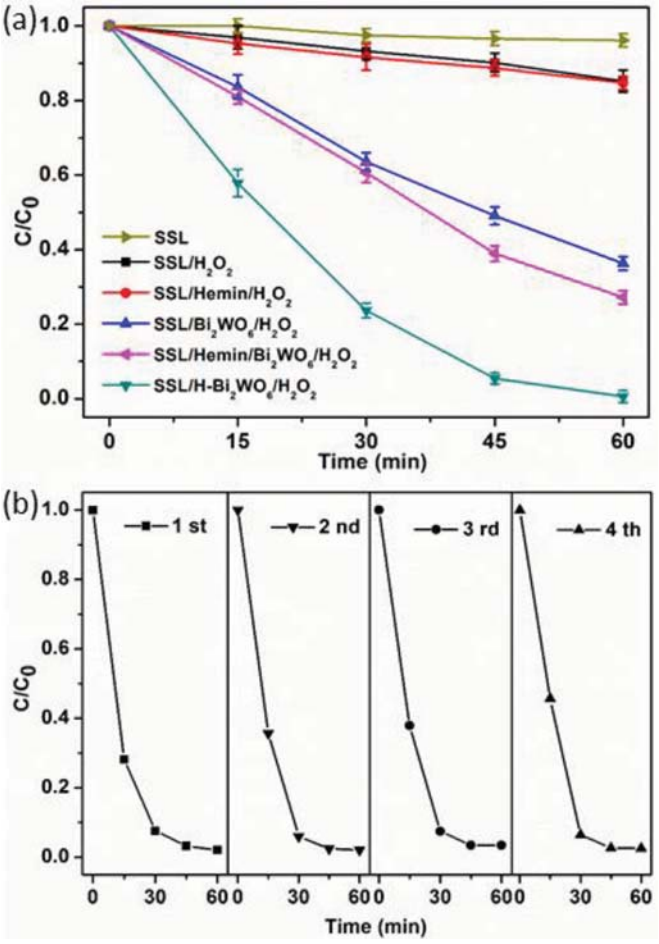

Fig. 5. (a) Photocatalytic activity analysis of different systems in the degradation of RhB; (b) cycling runs in the degradation of RhB through SSL/H-Bi_2WO_6/H_2O_2 process.

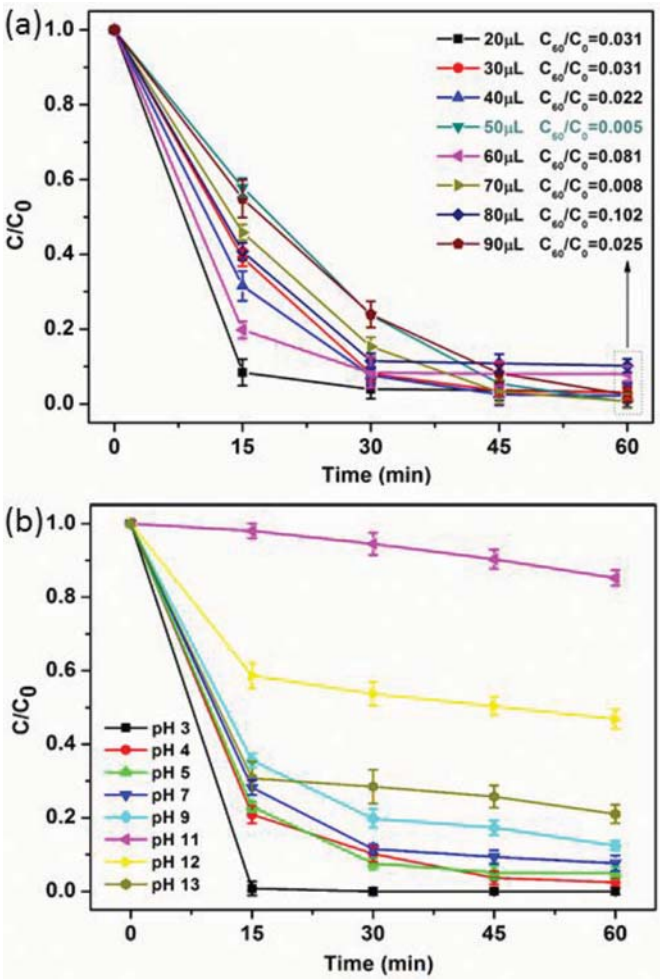

Fig. 6. (a) Effect of H_2O_2 in the SSL/H-Bi_2WO_6/H_2O_2 process; (b) effect of pH in the SSL/H-Bi_2WO_6/H_2O_2 process.

in RhB degradation (Fig. 5b), suggesting that H-Bi_2WO_6 has good photostability. Besides, the ability to deep mineralize organics is a key evaluation criterion for pollutant treatment. This work used TOC analysis to measure the mineralization for RhB. The removal of TOC in RhB aqueous solution achieved above 70% of TOC after 3 h SSL irradiation (Fig. S4). The result demonstrated that SSL/H-Bi_2WO_6/H_2O_2 process exhibited high photocatalytic activity in RhB degradation with a favourable mineralization ability.

3.3.3. Effect of initial H_2O_2 concentrations

Effect of initial H_2O_2 concentrations was explored on the RhB degradation over SSL/H-Bi_2WO_6/H_2O_2 process. As illustrated in Fig. 6a, all the experiments with a small amount of initial H_2O_2 concentrations ranging from 0.2–0.9‰ (in volume) showed an efficient degradation on RhB. Furthermore, the degradation efficiency of RhB increased with the increase of initial H_2O_2 concentrations, and optimized at 0.5‰ in volume. This is because a lower H_2O_2 concentration cannot generate enough ·OH radicals, while a higher H_2O_2 concentration would retard the photocatalytic Fenton-like process caused by the competition by excess H_2O_2 with RhB for ·OH radicals, generating weaker ·OOH radicals (Eq. (1)) and having a negative impact on RhB degradation.

$$\cdot OH + H_2O_2 \rightarrow \cdot OOH + H_2O \quad (1)$$

3.3.4. Effect of pH

Effect of pH varying from 3.0–13.0 on the photocatalytic degradation of RhB over SSL/H-Bi_2WO_6/H_2O_2 process was also explored.

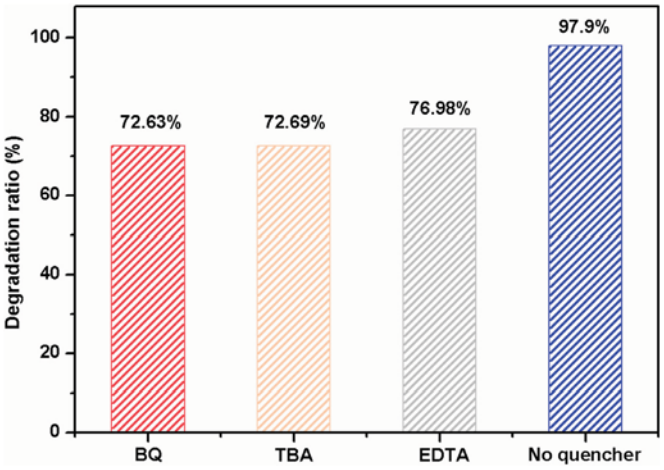

Fig. 7. Scavenger tests of SSL/H-Bi_2WO_6/H_2O_2 process.

As shown in Fig. 6b, when pH was below 9, the degradation of RhB is efficient. This is because the surface charge of the as-prepared catalysts became increasingly positive as the pH decreased resulting in increasingly stronger electrostatic repulsion with RhB, and the acid environment is beneficial for Fenton-like process. The degradation efficiency decreased when pH located at 11, because the negatively charged photocatalyst surface prevented the sorption of hydroxide ions, thus reducing the formation of hydroxyl radicals. However, the degradation efficiency has an increasing trend with the pH increasing from 12.0 to 13.0. This increasing trend might be attributed to the surface charge variations of RhB adsorbed onto H-Bi_2WO_6 [58]. And a system with high OH^- content can affect the stability of H_2O_2, then accelerate the generation of ·OH. The above results showed that SSL/H-Bi_2WO_6/H_2O_2 process possessed enhanced pH tolerance.

3.4. Proposed photocatalytic mechanism in organic dyes removal

To understand the mechanism of SSL/H-Bi_2WO_6/H_2O_2 process, scavenger tests were performed to evaluate the contribution of the specific free radical species to photocatalytic degradation. BQ, TBA and EDTA-2Na were used as the scavengers of $\cdot O_2^-$, ·OH and h^+, respectively [62]. As shown in Fig. 7, it can be found that the photocatalytic performance of SSL/H-Bi_2WO_6/H_2O_2 process decrease after adding these scavengers. The activity was inhibited by BQ, TBA and EDTA-2Na, and the degradation rate was reduced from 97.9% to 72.6%, 72.7% and 76.9%, respectively. The result implies the $\cdot O_2^-$, ·OH and h^+ should have an influence on the photocatalytic activity of the SSL/H-Bi_2WO_6/H_2O_2 process. Meanwhile, ESR with 5,5-dimethyl-1-pyrroline N-oxide (DMPO) in aqueous solution was performed to further confirm the reactive oxygen species [63]. There is no obvious ·OH and $\cdot O_2^-$ signal in the dark, but an increasing trend can be observed after irradiation (Fig. 8), suggesting that ·OH and $\cdot O_2^-$were formed in the SSL/H-Bi_2WO_6/H_2O_2 process. But according to the literature [64–67], the photogenerated electrons on CB of Bi_2WO_6 can easily transfer to the adsorbed oxygen molecules to form $\cdot O_2^-$, while ·OH cannot be directly generated via the hole on VB of Bi_2WO_6. Presumably, the ·OH detected in Fig. 8a with four obvious signals (1:2:2:1) were generated from the decomposition of H_2O_2 added after the dark reaction or the multi-step reduction of $\cdot O_2^-$ [68–74].

Except the contribution of $\cdot O_2^-$, ·OH, and h^+, end-on Fe(IV)=O species formed by the reaction of hemin-Fe(III) in H-Bi_2WO_6 with H_2O_2 might also played a role in the photodegradation of RhB [45]. The hydrogen peroxide O–O bond can be cleaved through homolysis or heterolysis, which is related to the conditions [75]. When the

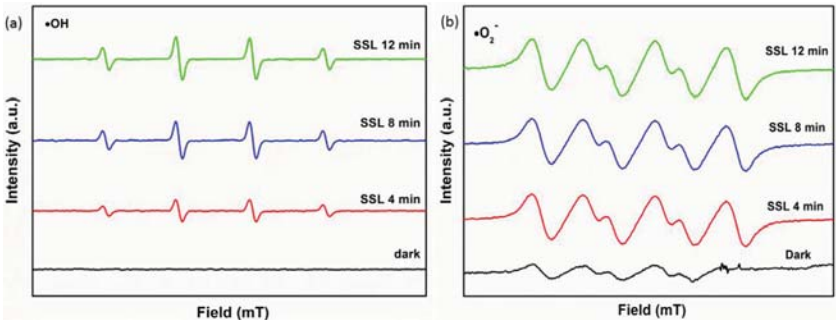

Fig. 8. ERS analysis of SSL/H-Bi_2WO_6/H_2O_2 process.

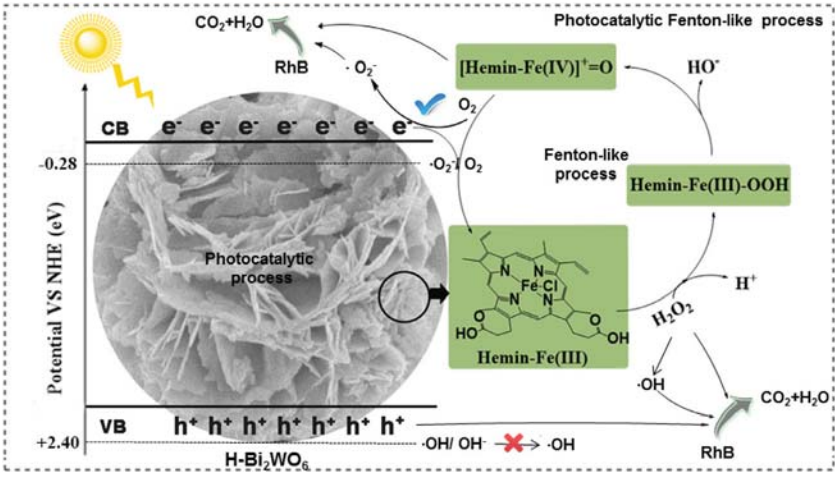

Fig. 9. Possible reaction mechanism over the H_2O_2 assisted H-Bi_2WO_6 photocatalyst under solar irradiation.

axial groups or substituent groups of hemin are electron acceptor, it is in the favour of hemolytic cleavage of the O–O band, whereas it is beneficial for the heterolytic cleavage of O–O bond when the axial groups or substituent groups of hemin are electron donators. In SSL/Bi_2WO_6/H_2O_2 process, Bi_2WO_6 under SSL irradiation is an electron donator, which will enhance the H_2O_2 heterolytic process and facilitate the formation of Fe(IV)=O active species. Fe(IV)=O are strong oxidative species that can also take part in the degradation of RhB.

Based on all the experimental results, a possible mechanism for the high photocatalytic activity and stability of the as-prepared H-Bi_2WO_6 is proposed in Fig. 9. Under SSL irradiation, H-Bi_2WO_6 absorbed efficient photons and then generated lots of electrons and hole with the assistance of H_2O_2. And there was a special association between chlorine ions of hemin and hydrated excess proton generated in SSL/H-Bi_2WO_6/H_2O_2 process, which had a positive effect on the photoinduced positive charge transportation from H-Bi_2WO_6 bridging oxygen to those of the amorphous layer [76]. Hemin acted as an electron shuttle that quickly transferred the photoelectrons from Bi_2WO_6 to combined oxygen molecules to form $\cdot O_2^-$ species [44,77,78]. Moreover, hemin reacted with added H_2O_2 to form Fe(IV)=O species for RhB degradation. Besides, ·OH generated from the decomposition of H_2O_2 and the hole left in VB of H-Bi_2WO_6 were powerful oxidants that can also degrade RhB directly.

4. Conclusions

In summary, SSL/H-Bi_2WO_6/H_2O_2 process was an effective method for degradation of synthetic organic dyes. Novel photocatalyst H-Bi_2WO_6 was successfully prepared via a facile one-step solvothermal method. The hemin particles were highly dispersed on the Bi_2WO_6 surface and they can effectively enhance the photocatalytic activity of Bi_2WO_6. This could be ascribed to two aspects: (i) hemin acted as an electron shuttle that transferred the photogenerated electrons from CB of Bi_2WO_6 to the surface to be trapped by dissolved molecular oxygen to form strong oxidative radicals $\cdot O_2^-$; (ii) hemin consumed the photoelectrons through the Fenton-like circulation with the assistance of trace H_2O_2. Moreover, H-Bi_2WO_6 disfavoured protons transfer to the bound oxygen species, funneling the O–O activation pathway to single-electron chemistry and the production of H_2O_2. Particularly, the photocatalytic Fenton-like method through SSL/H-Bi_2WO_6/H_2O_2 process presented in this work well meets the requirements of 21st century green development: environment-friendly materials, sustainable energy and efficient economy.

Acknowledgments

This study was financially supported by the Program for the National Natural Science Foundation of China (51579098, 51779090, 51709101, 51278176, 51408206, 51521006), Science and Technology Plan Project of Hunan Province (2017SK2243, 2016RS3026), the National Program for Support of Top-Notch Young Professionals of China (2014), the Program for New Century Excellent Talents in University (NCET-13-0186), the Program for Changjiang Scholars and Innovative Research Team in University (IRT-13R17), and the Fundamental Research Funds for the Central Universities (531107050978, 531107051080).

Supplementary materials

Supplementary material associated with this article can be found, in the online version, at doi:10.1016/j.jtice.2018.06.037.

References

[1] Huang D, Xue W, Zeng G, Wan J, Chen G, Huang C, Zhang C, Cheng M, Xu P. Immobilization of Cd in river sediments by sodium alginate modified nanoscale zero-valent iron: impact on enzyme activities and microbial community diversity. Water Res 2016;106:15–25.

[2] Tang W-W, Zeng G-M, Gong J-L, Liang J, Xu P, Zhang C, Huang B-B. Impact of humic/fulvic acid on the removal of heavy metals from aqueous solutions using nanomaterials: a review. Sci Total Environ 2014;468:1014–27.

[3] Liang J, Yang Z, Tang L, Zeng G, Yu M, Li X, Wu H, Qian Y, Li X, Luo Y. Changes in heavy metal mobility and availability from contaminated wetland soil remediated with combined biochar-compost. Chemosphere 2017;181:281–8.

[4] Wu H, Lai C, Zeng G, Liang J, Chen J, Xu J, Dai J, Li X, Liu J, Chen M. The interactions of composting and biochar and their implications for soil amendment and pollution remediation: a review. Crit Rev Biotechnol 2017;37:754–64.

[5] Yang C, Chen H, Zeng G, Yu G, Luo S. Biomass accumulation and control strategies in gas biofiltration. Biotechnol Adv 2010;28:531–40.

[6] Yi H, Zeng G, Lai C, Huang D, Tang L, Gong J, Chen M, Xu P, Wang H, Cheng M, Zhang C, Xiong W. Environment-friendly fullerene separation methods. Chem Eng J 2017;330:134–45.

[7] Gong J-L, Wang B, Zeng G-M, Yang C-P, Niu C-G, Niu Q-Y, Zhou W-J, Liang Y. Removal of cationic dyes from aqueous solution using magnetic multi-wall carbon nanotube nanocomposite as adsorbent. J Hazard Mater 2009;164:1517–22.

[8] Tan X, Liu Y, Zeng G, Wang X, Hu X, Gu Y, Yang Z. Application of biochar for the removal of pollutants from aqueous solutions. Chemosphere 2015;125:70–85.

[9] Deng J-H, Zhang X-R, Zeng G-M, Gong J-L, Niu Q-Y, Liang J. Simultaneous removal of Cd (II) and ionic dyes from aqueous solution using magnetic graphene oxide nanocomposite as an adsorbent,. Chem Eng J 2013;226:189–200.

[10] Xu P, Zeng GM, Huang DL, Lai C, Zhao MH, Wei Z, Li NJ, Huang C, Xie GX. Adsorption of Pb (II) by iron oxide nanoparticles immobilized Phanerochaete chrysosporium: equilibrium, kinetic, thermodynamic and mechanisms analysis. Chem Eng J 2012;203:423–31.

[11] Zhang C, Lai C, Zeng G, Huang D, Yang C, Wang Y, Zhou Y, Cheng M. Efficacy of carbonaceous nanocomposites for sorbing ionizable antibiotic sulfamethazine from aqueous solution. Water Res 2016;95:103–12.

[12] Long F, Gong J-L, Zeng G-M, Chen L, Wang X-Y, Deng J-H, Niu Q-Y, Zhang H-Y, Zhang X-R. Removal of phosphate from aqueous solution by magnetic Fe–Zr binary oxide. Chem Eng J 2011;171:448–55.

[13] Cheng M, Zeng G, Huang D, Lai C, Xu P, Zhang C, Liu Y. Hydroxyl radicals based advanced oxidation processes (AOPs) for remediation of soils contaminated with organic compounds: a review. Chem Eng J 2016;284:582–98.

[14] Cheng Y, He H, Yang C, Zeng G, Li X, Chen H, Yu G. Challenges and solutions for biofiltration of hydrophobic volatile organic compounds. Biotechnol Adv 2016;34:1091–102.

[15] Ming C, Xu P, Zeng G, Yang C, Huang D, Zhang J. Bioremediation of soils contaminated with polycyclic aromatic hydrocarbons, petroleum, pesticides, chlorophenols and heavy metals by composting: applications, microbes and future research needs. Biotechnol Adv 2015;33:745–55.

[16] Gong X, Huang D, Liu Y, Zeng G, Wang R, Wan J, Zhang C, Cheng M, Qin X, Xue W. Stabilized nanoscale zerovalent iron mediated cadmium accumulation and oxidative damage of Boehmeria nivea (L.) Gaudich cultivated in cadmium contaminated sediments. Environ Sci Technol 2017;51:11308–16.

[17] Huang D, Liu L, Zeng G, Xu P, Huang C, Deng L, Wang R, Wan J. The effects of rice straw biochar on indigenous microbial community and enzymes activity in heavy metal-contaminated sediment. Chemosphere 2017;174:545–53.

[18] Zhang Y, Zeng GM, Tang L, Chen J, Zhu Y, He XX, He Y. Electrochemical sensor based on electrodeposited graphene-Au modified electrode and nanoAu carrier amplified signal strategy for attomolar mercury detection. Anal Chem 2015;87:989–96.

[19] Lai C, Wang M-M, Zeng G-M, Liu Y-G, Huang D-L, Zhang C, Wang R-Z, Xu P, Cheng M, Huang C, Wu H-P, Qin L. Synthesis of surface molecular imprinted TiO_2/graphene photocatalyst and its highly efficient photocatalytic degradation of target pollutant under visible light irradiation. Appl Surf Sci 2016;390:368–76.

[20] Wang H, Yuan X, Wang H, Chen X, Wu Z, Jiang L, Xiong W, Zeng G. Facile synthesis of Sb_2S_3/ultrathin g-C_3N_4 sheets heterostructures embedded with g-C_3N_4 quantum dots with enhanced NIR-light photocatalytic performance. Appl Catal B Environ 2016;193:36–46.

[21] Huang D, Hu C, Zeng G, Cheng M, Xu P, Gong X, Wang R, Xue W. Combination of Fenton processes and biotreatment for wastewater treatment and soil remediation. Sci Total Environ 2017;574:1599–610.

[22] Cheng M, Zeng G, Huang D, Lai C, Liu Y, Xu P, Zhang C, Wan J, Hu L, Xiong W, Zhou C. Salicylic acid-methanol modified steel converter slag as heterogeneous Fenton-like catalyst for enhanced degradation of alachlor. Chem Eng J 2017;327:686–93.

[23] Clarizia L, Russo D, Di Somma I, Marotta R, Andreozzi R. Homogeneous photo-Fenton processes at near neutral pH: a review. Appl Catal B Environ 2017;209:358–71.

[24] Martín-Sómer M, Vega B, Pablos C, van Grieken R, Marugán J. Wavelength dependence of the efficiency of photocatalytic processes for water treatment. Appl Catal B Environ 2018;221:258–65.

[25] Yang T, Peng J, Zheng Y, He X, Hou Y, Wu L, Fu X. Enhanced photocatalytic ozonation degradation of organic pollutants by ZnO modified TiO_2 nanocomposites. Appl Catal B Environ 2018;221:223–34.

[26] Ortega-Liebana M, Hueso J, Larrea A, Sebastian V, Santamaria J. Feroxyhyte nanoflakes coupled to up-converting carbon nanodots: a highly active, magnetically recoverable, Fenton-like photocatalyst in the visible-NIR range. Chem Commun 2015;51:16625–8.

[27] Almeida LC, Silva BF, Zanoni MVB. Combined photoelectrocatalytic/electro-Fenton process using a Pt/TiO_2NTs photoanode for enhanced degradation of an azo dye: a mechanistic study. J Electroanal Chem 2014;734:43–52.

[28] Li Y, Ouyang S, Xu H, Wang X, Bi Y, Zhang Y, Ye J. Constructing solid–gas-interfacial fenton reaction over alkalinized-C_3N_4 photocatalyst to achieve apparent quantum yield of 49% at 420 nm. J Am Chem Soc 2016;138:13289–97.

[29] Guo S, Zhu Y, Yan Y, Min Y, Fan J, Xu Q. Holey structured graphitic carbon nitride thin sheets with edge oxygen doping via photo-Fenton reaction with enhanced photocatalytic activity. Appl Catal, B 2016;185:315–21.

[30] Yoon M, Oh Y, Hong S, Lee JS, Boppella R, Kim SH, Marques Mota F, Kim SO, Kim DH. Synergistically enhanced photocatalytic activity of graphitic carbon nitride and WO_3 nanohybrids mediated by photo-Fenton reaction and H_2O_2. Appl Catal B Environ 2017;206:263–70.

[31] Hori H, Takase M, Takashima M, Amano F, Shibayama T, Ohtani B. Mechanism of formation, structural characteristics and photocatalytic activities of hierarchical-structured bismuth-tungstate particles. Catal Today 2018;300:99–111.

[32] Lee W-LW, Huang S-T, Chang J-L, Chen J-Y, Cheng M-C, Chen C-C. Photodegradation of CV over nanocrystalline bismuth tungstate prepared by hydrothermal synthesis. J Mol Catal A Chem 2012;361–362:80–90.

[33] Liao Y-HB, Wang JX, Lin J-S, Chung W-H, Lin W-Y, Chen C-C. Synthesis, photocatalytic activities and degradation mechanism of Bi2WO6 toward crystal violet dye. Catal Today 2011;174:148–59.

[34] Zheng H, Guo W, Li S, Yin R, Wu Q, Feng X, Ren N, Chang J-S. Surfactant (CTAB) assisted flower-like Bi_2WO_6 through hydrothermal method: Unintentional bromide ion doping and photocatalytic activity. Catal Commun 2017;88:68–72.

[35] Zhu Y, Wang Y, Ling Q, Zhu Y. Enhancement of full-spectrum photocatalytic activity over BiPO4/Bi_2WO_6 composites. Appl Catal B Environ 2017;200:222–9.

[36] Lee Y-H, Dai Y-M, Fu J-Y, Chen C-C. A series of bismuth-oxychloride/bismuth-oxyiodide/graphene-oxide nanocomposites: Synthesis, characterization, and photcatalytic activity and mechanism. Mol Catal 2017;432:196–209.

[37] Chen C-C, Chen W-C, Chiou M-R, Chen S-W, Chen YY, Fan H-J. Degradation of crystal violet by an FeGAC/H_2O_2 process. J Hazard Mater 2011;196:420–5.

[38] Fan H-J, Huang S-T, Chung W-H, Jan J-L, Lin W-Y, Chen C-C. Degradation pathways of crystal violet by Fenton and Fenton-like systems: Condition optimization and intermediate separation and identification. J Hazard Mater 2009;171:1032–44.

[39] Xu P, Zeng GM, Huang DL, Feng CL, Hu S, Zhao MH, Lai C, Wei Z, Huang C, Xie GX, Liu ZF. Use of iron oxide nanomaterials in wastewater treatment: a review. Sci Total Environ 2012;424:1–10.

[40] Liang S, Jia Z, Zhang W, Li X, Wang W, Lin H, Zhang L. Ultrafast activation efficiency of three peroxides by $Fe_{78}Si_9B_{13}$ metallic glass under photo-enhanced catalytic oxidation: a comparative study. Appl Catal B Environ 2018;221:108–18.

[41] Xue W, Huang D, Zeng G, Wan J, Zhang C, Xu R, Cheng M, Deng R. Nanoscale zero-valent iron coated with rhamnolipid as an effective stabilizer for immobilization of Cd and Pb in river sediments. J Hazard Mater 2018;341:381–9.

[42] Xue T, Jiang S, Qu Y, Su Q, Cheng R, Dubin S, Chiu C-Y, Kaner R, Huang Y, Duan X. Graphene-supported hemin as a highly active biomimetic oxidation catalyst. Angew Chem Int Ed 2012;51:3822–5.

[43] Jiang B, Yao Y, Xie R, Dai D, Lu W, Chen W, Zhang L. Enhanced generation of reactive oxygen species for efficient pollutant elimination catalyzed by hemin based on persistent free radicals. Appl Catal, B 2016;183:291–7.

[44] Li Z, Tian B, Zhen W, Wu Y, Lu G. Inhibition of hydrogen and oxygen recombination using oxygen transfer reagent hemin chloride in Pt/TiO_2 dispersion for photocatalytic hydrogen generation. Appl Catal B Environ 2017;203:408–15.

[45] Chen X, Lu W, Xu T, Li N, Qin D, Zhu Z, Wang G, Chen W. A bio-inspired strategy to enhance the photocatalytic performance of g-C_3N_4 under solar irradiation by axial coordination with hemin. Appl Catal B Environ 2017;201:518–26.

[46] Zhao Y, Zhang Y, Liu A, Wei Z, Liu S. Construction of three-dimensional hemin-functionalized graphene hydrogel with high mechanical stability and adsorption capacity for enhancing photodegradation of methylene blue. ACS Appl Mater Interfaces 2017;9:4006–14.

[47] Da Silva ES, Moura NMM, Neves MGPMS, Coutinho A, Prieto M, Silva CG, Faria JL. Novel hybrids of graphitic carbon nitride sensitized with free-base meso-tetrakis(carboxyphenyl) porphyrins for efficient visible light photocatalytic hydrogen production. Appl Catal, B 2018;221:56–69.

[48] Yao Y, Mao Y, Huang Q, Wang L, Huang Z, Lu W, Chen W. Enhanced decomposition of dyes by hemin-ACF with significant improvement in pH tolerance and stability. J Hazard Mater 2014;264:323–31.

[49] Zhang Q, Li C, Li T. Rapid photocatalytic decolorization of methylene blue using high photon flux UV/TiO_2/H_2O_2 process. Chem Eng J 2013;217:407–13.

[50] Lei P, Chen C, Yang J, Wanhong M, Zhao J, Zang L. Degradation of dye pollutants by immobilized polyoxometalate with H_2O_2 under visible-light irradiation. Environ Sci Technol 2005;39:8466–74.

[51] Chen M, Chu W. H_2O_2 assisted degradation of antibiotic norfloxacin over simulated solar light mediated Bi_2WO_6: kinetics and reaction pathway. Chem Eng J 2016;296:310–18.

[52] Cheng M, Zeng G, Huang D, Lai C, Xu P, Zhang C, Liu Y, Wan J, Gong X, Zhu Y. Degradation of atrazine by a novel Fenton-like process and assessment the influence on the treated soil. J Hazard Mater 2016;312:184–91.

[53] Huang X, Hou X, Zhao J, Zhang L. Hematite facet confined ferrous ions as high efficient Fenton catalysts to degrade organic contaminants by lowering H_2O_2 decomposition energetic span. Appl Catal B Environ 2016;181:127–37.
[54] Li G, Zhang D, Yu JC, Leung MKH. An efficient bismuth tungstate visible–light-driven photocatalyst for breaking down nitric oxide. Environ Sci Technol 2010;44:4276–81.
[55] Qamar M, Khan A. Mesoporous hierarchical bismuth tungstate as a highly efficient visible-light-driven photocatalyst. RSC Adv 2014;4:9542–50.
[56] Zou J-P, Ma J, Luo J-M, Yu J, He J, Meng Y, Luo Z, Bao S-K, Liu H-L, Luo S-L, Luo X-B, Chen T-C, Suib SL. Fabrication of novel heterostructured few layered WS_2-Bi_2WO_6/$Bi_{3.84}W_{0.16}O_{6.24}$ composites with enhanced photocatalytic performance. Appl Catal B Environ 2015;179:220–8.
[57] Zhang MM, Zhu YY, Li WJ, Wang FZ, Li HD, Liu XT, Zhang WW, Ren CJ. Double Z-scheme system of silver bromide@bismuth tungstate/tungsten trioxide ternary heterojunction with enhanced visible-light photocatalytic activity. J Colloid Interface Sci 2018;509:18–24.
[58] Tang L, Wang J, Zeng G, Liu Y, Deng Y, Zhou Y, Tang J, Wang J, Guo Z. Enhanced photocatalytic degradation of norfloxacin in aqueous Bi_2WO_6 dispersions containing nonionic surfactant under visible light irradiation. J Hazard Mater 2016;306:295–304.
[59] Dumrongrojthanath P, Thongtem T, Phuruangrat A, Thongtem S. Hydrothermal synthesis of Bi_2WO_6 hierarchical flowers with their photonic and photocatalytic properties. Superlattices Microstruct 2013;54:71–7.
[60] Yao Y, Mao Y, Huang Q, Wang L, Huang Z, Lu W, Chen W. Enhanced decomposition of dyes by hemin-ACF with significant improvement in pH tolerance and stability. J Hazard Mater 2014;264:323–31.
[61] Zhou C, Lai C, Huang D, Zeng G, Zhang C, Cheng M, Hu L, Wan J, Xiong W, Wen M. Highly porous carbon nitride by supramolecular preassembly of monomers for photocatalytic removal of sulfamethazine under visible light driven. Appl Catal, B 2017;220:202–10.
[62] Shang Y, Chen X, Liu W, Tan P, Chen H, Wu L, Ma C, Xiong X, Pan J. Photocorrosion inhibition and high-efficiency photoactivity of porous g-C_3N_4/Ag_2CrO_4 composites by simple microemulsion-assisted co-precipitation method. Appl Catal B Environ 2017;204:78–88.
[63] Chen F, Yang Q, Wang Y, Zhao J, Wang D, Li X, Guo Z, Wang H, Deng Y, Niu C. Novel ternary heterojunction photcocatalyst of Ag nanoparticles and g-C_3N_4 nanosheets co-modified $BiVO_4$ for wider spectrum visible-light photocatalytic degradation of refractory pollutant. Appl Catal B Environ 2017;205:133–47.
[64] Huang Y, Kang S, Yang Y, Qin H, Ni Z, Yang S, Li X. Facile synthesis of Bi/Bi_2WO_6 nanocomposite with enhanced photocatalytic activity under visible light. Appl Catal B Environ 2016;196:89–99.
[65] Wang D, Guo L, Zhen Y, Yue L, Xue G, Fu F. AgBr quantum dots decorated mesoporous Bi_2WO_6 architectures with enhanced photocatalytic activities for methylene blue. J Mater Chem A 2014;2:11716–27.
[66] Liu Y, Wei B, Xu L, Gao H, Zhang M. Generation of oxygen vacancy and OH radicals: a comparative study of Bi_2WO_6 and Bi_2WO_6−x nanoplates. ChemCatChem 2015;7:4076–84.
[67] Ren J, Wang W, Sun S, Zhang L, Chang J. Enhanced photocatalytic activity of Bi_2WO_6 loaded with Ag nanoparticles under visible light irradiation. Appl Catal B Environ 2009;92:50–5.
[68] Jiang Y-R, Lin H-P, Chung W-H, Dai Y-M, Lin W-Y, Chen C-C. Controlled hydrothermal synthesis of BiOxCly/BiOmIn composites exhibiting visible-light photocatalytic degradation of crystal violet. J Hazard Mater 2015;283:787–805.
[69] Chou S-Y, Chen C-C, Dai Y-M, Lin J-H, Lee WW. Novel synthesis of bismuth oxyiodide/graphitic carbon nitride nanocomposites with enhanced visible-light photocatalytic activity. RSC Adv 2016;6:33478–91.
[70] Yang C-T, Lee WW, Lin H-P, Dai Y-M, Chi H-T, Chen C-C. A novel heterojunction photocatalyst, Bi_2SiO_5/gC_3N_4: synthesis, characterization, photocatalytic activity, and mechanism. RSC Adv 2016;6:40664–75.
[71] Liu F-Y, Jiang Y-R, Chen C-C, Lee WW. Novel synthesis of $PbBiO_2Cl$/BiOCl nanocomposite with enhanced visible-driven-light photocatalytic activity. Catal Today 2018;300:112–23.
[72] Chou S-Y, Chung W-H, Chen L-W, Dai Y-M, Lin W-Y, Lin J-H, Chen C-C. A series of BiOxly/GO photocatalysts: synthesis, characterization, activity, and mechanism. RSC Adv 2016;6:82743–58.
[73] Lin H-P, Chen C-C, Lee WW, Lai Y-Y, Chen J-Y, Chen Y-Q, Fu J-Y. Synthesis of a SrFeO3-x/g-C3N4 heterojunction with improved visible-light photocatalytic activities in chloramphenicol and crystal violet degradation. RSC Adv 2016;6:2323–36.
[74] Leaf-nosed bat. Encyclopædia britannica. Encyclopædia Britannica Online; 2009.
[75] Nam W, Han HJ, Oh S-Y, Lee YJ, Choi M-H, Han S-Y, Kim C, Woo SK, Shin W. New Insights into the mechanisms of O−O bond cleavage of hydrogen peroxide and tert-alkyl hydroperoxides by iron (III) porphyrin complexes. J Am Chem Soc 2000;122:8677–84.
[76] Torralvo M, Sanz J, Sobrados I, Soria J, Garlisi C, Palmisano G, Çetinkaya S, Yurdakal S, Augugliaro V. Anatase photocatalyst with supported low crystalline TiO_2: the influence of amorphous phase on the activity. Appl Catal B Environ 2018;221:140–51.
[77] Zhang Y, Zhang N, Tang Z-R, Xu Y-J. Identification of Bi_2WO_6 as a highly selective visible-light photocatalyst toward oxidation of glycerol to dihydroxyacetone in water. Chem Sci 2013;4:1820–4.
[78] Houas A, Lachheb H, Ksibi M, Elaloui E, Guillard C, Herrmann J-M. Photocatalytic degradation pathway of methylene blue in water. Appl Catal B 2001;31:145–57.